Investigation of Fatigue Strength of Root of Lap Fillet Welds of Thin Sheet and Improvement Method

Matsuda, Kazuki
Kyushu University

Yonezawa, Takayuki
Nippon Steel Corporation

出版情報：Theoretical and Applied Fracture Mechanics. 122 (103667), 2022-12. Elsevier
バージョン：
権利関係：

Title

Investigation of Fatigue Strength of Root of Lap Fillet Welds of Thin Sheet and Improvement Method

Kazuki Matsuda*

Kyushu University, 744 Motooka, Nishi-ku, Fukuoka, 819-0395, Japan

(Formerly Nippon Steel Corporation)

E-mail: matsuda@nams.kyushu-u.ac.jp

Takayuki Yonezawa

Nippon Steel Corporation, 20-1 Shintomi, Futtsu, Chiba prefecture, 293-8511, Japan

E-mail: yonezawa.94m.takayuki@jp.nipponsteel.com

*corresponding author

Abstract

This study investigates the dominant factors of fatigue strength at the root of thin-sheet lap fillet arc welds, which are frequently used in automobile chassis components. A method to improve the root fatigue strength was investigated. The direction of fatigue crack propagation at the root coincided with the direction of maximum circumferential stress range. The circumferential stress was reduced by increasing the distance from the toe to the root (penetration width). Fatigue strength originating from the root was improved in welded joints where the penetration width was increased by adjusting the welding aim point and heat input.

Keywords

Thin arc weld; Root fatigue strength; Thin steel sheet; Automobile chassis

Nomenclature

b [mm]: width of the center of fatigue test specimen

h [mm]: thickness of the steel sheet

$K_{\theta max}$ [MPa√m]: maximum value of stress intensity factor for mode I

M [N・mm]: bending moment at fatigue test

Z [mm^3]: section modulus

σ [MPa]: bending stress

$\Delta K_{\theta th}$ [MPa√m]: threshold of stress intensity factor range for mode I

$\Delta\sigma$ [MPa]: stress range

1. Introduction

Since rigidity and high joint strength are required for automotive chassis components, arc welding is frequently used for joining [1]. Improving the fatigue strength of joints is an important issue. In many cases, lap fillet joints are used as the joint type in automotive chassis components. The fatigue crack initiation point is usually at the toe. The root section is generally not designed to be subjected to tensile stress because of its high geometrical stress concentration. The fatigue strength at a toe is influenced by stress concentration at the toe [2], weld metal strength [3], and micro irregularities on the surface of the weld metal [4, 5]. These factors can help improve the fatigue strength with the toe as the crack initiation point but not the fatigue strength of the root. Therefore, there is a concern that fatigue failure will eventually occur at the root as the strength at the toe

is improved. Although the fatigue strength of the toe can be improved by post-treatment [6, 7], the fatigue strength of the root is not improved.

Various fatigue evaluation methods have been proposed for the root of arc welded joints [8]. The simplest method is to use nominal stress, but this method cannot consider secondary bending stress due to misalignment. Fricke, et al. [9] evaluated the fatigue strength of the root simply by analyzing the structural stress using a relatively coarse finite element model. Meneghetti [10] evaluated the fatigue strength of the root by extending the peak stress method (PSM) to mode I, II and III loading. Song, et al. [11] evaluated the fatigue strength of the root using the averaged strain energy density (SED) for load-carrying cruciform welded joints. Although the fatigue strength of the weld root has been focused on due to the high stress concentration, a simple method to improve it has not been reported.

In this study, the factors dominating the fatigue strength of the root of lap fillet arc welds were investigated by finite element (FE) method and fatigue tests. In addition, a method to improve the fatigue strength of welds initiating from the root was proposed and investigated by fatigue tests.

2. Calculation

Stress analysis of the root section of a lap fillet weld is performed. The analysis code used was MSC Marc2018. The geometry analyzed is a lap fillet weld of a 2.9 mm-thin steel sheet as shown in Figure 1. The FE model is a two-dimensional model. The analysis was performed under plane strain conditions. The element type is a four-node quadrilateral full integral element. The root is defined as the position where the boundary between the upper and lower sheets intersects the weld metal. The distance from the toe to the root is

defined as the penetration width. Two models (M6 and M8) with 6 mm and 8 mm penetration widths were created to investigate the effect of penetration width on fatigue strength. The model geometry (Figure 1) was mesh-divided, as shown in Figure 2. The thickness of the FE model was varied according to the width of the specimen as described below (**Figure 5**). This is an elastic stress analysis, and Young's modulus and Poisson's ratio were set to 206 GPa and 0.3, respectively.

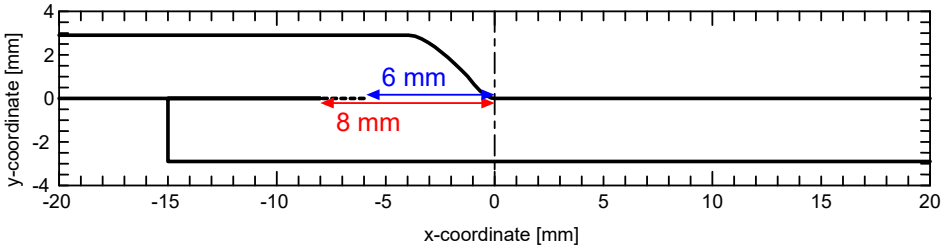

Figure 1. FE Model outline.

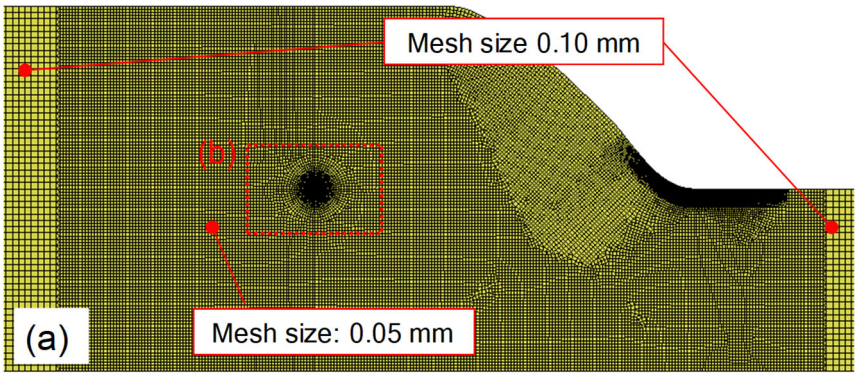

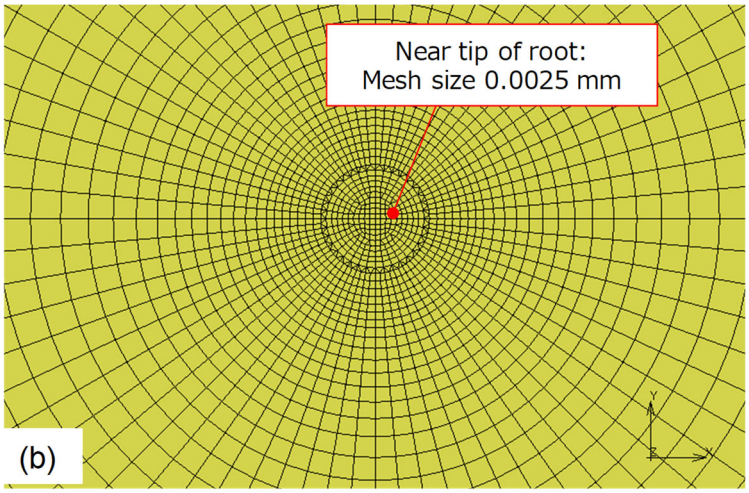

Figure 2. FE model: (a) Weld metal part, (b) Near the root.

A schematic diagram of the boundary conditions set for the model is shown in Figure 3. The displacements in the x- and y-directions at one end were fixed, and a bending moment was applied at the other end. The bending moment M was divided by the section modulus Z to convert it into a bending stress σ. The section modulus Z was obtained by using the relation $Z = bh^2/6$, where b is specimen width and h is the thickness of the toe section. Since the stress range is important for fatigue strength, stress analysis was performed for bending stresses of +1 MPa (root closure) and -1 MPa (root opening). The contact between upper and lower sheets has been simulated.

Figure 3. Schematic of boundary conditions.

3. Materials and Methods

Lab- hot rolled steel sheets with a thickness of 2.9 mm and tensile strength of 506 MPa were use along with general-purpose solid welding wires of 490 MPa grade steel and 1.2 mm diameter.

The joint type is a lap fillet joint. A schematic illustration of the welding is shown in Figure 4. The overlap between the upper and lower sheets was 10 mm. The linear distance from the contact tip to the base metal was 15 mm and the torch angle was 60°. Arc welding was performed under the two conditions shown in Table 1, in which the aiming position and heat input were varied to change the penetration width. The target values of the penetration width were 6 mm and 8 mm for S and L, respectively; further, for L, the welding target position was set on the upper plate side and the heat input was increased to increase the penetration width while suppressing melt drop. A cross-sectional sample was taken from the obtained welded part and observed using optical microscopy.

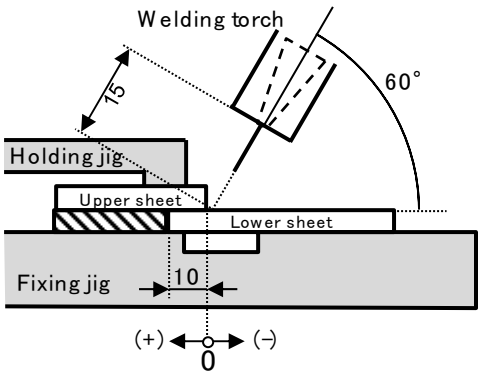

Figure 4. Schematic of lap fillet arc welding.

Table 1. Welding conditions.

Condition		S	L
Current	A	210	230
Voltage	V	24.1	28.3
Welding speed	m/min	0.8	
Position of weld	mm	-0.5	1.0
Shield gas		Ar +20%CO_2	
Mode		D.C. pulse	

The geometry of the specimen for fatigue test is shown in Figure 5~~Figure 5~~. The fatigue tests in this study were conducted as-welded. A Schenck-type fatigue test machine was used. A displacement-controlled plane bending loading (R = 0.1, direction of root opening) was used for the fatigue test. Initially, a stress ratio of R = -1 was implemented, but some specimens developed fatigue cracks from the toe, so the stress ratio was set to R = 0.1 in the direction of the root opening. The specimen was fixed at one end and the out-of-plane displacement was loaded at the other end. The load cell is located at the fixed end. The bending moment was calculated by multiplying the reaction force by the length of the specimen. The loading frequency is 25 Hz. Failure was defined by a drop in the bending moment to below 50 % from the initial moment. The stress range $\Delta\sigma$ is the difference between the maximum stress and the minimum stress. The maximum and minimum stresses are based on the bending stress of the surface σ, which was calculated using the relation $\sigma = 6\,M/bt^2$, where b, t, and M are the width of the center of the specimen, sheet thickness, and bending moment, respectively. The fatigue limit was defined as the non-fracture stress range at 10^7 cycles.

After the fatigue test, to investigate the direction of fatigue crack propagation at root, the microcracks were examined in the specimen that had not failed at 10^7 cycles.

The observation position was the cross section of the center of the specimen.

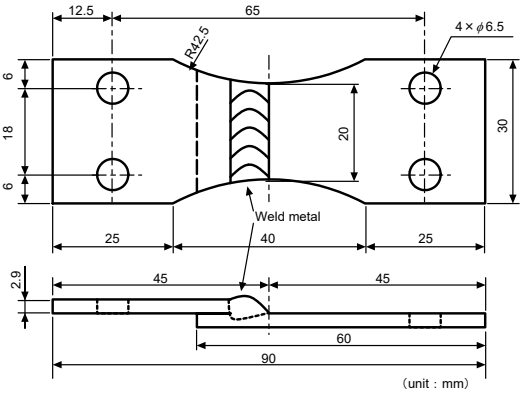

Figure 5. Geometry of the specimen for the fatigue test.

4. Results

4.1 FE Analysis

Polar coordinates were taken with the root tip as the origin. The bottom edge of the upper sheet was set at 0° and angled clockwise; the top edge of the lower sheet was set at 360°. **Figure 6** shows a contour plot of the stress components around the root at +1 MPa and -1 MPa bending stress. A circle with a radius of 0.05 mm was drawn around the root tip as a guide to the image area. First, (a) radial stress indicates that tensile and compressive stresses occur in the left side (0 ~ 90° and 270 ~ 360°) of the root tip, corresponding to the bending deformation of the entire specimen. In contrast, on the right side (90 ~ 270°), large tensile stresses occur at -1 MPa, when the root opens. Next, (b) circumferential stress shows that for (b-i), at +1 MPa, compression occurs on the upper side and tension on the lower side. This is considered to be because of the bending deformation behavior of the specimen. From (b-ii), it can be seen that at -1 MPa, a large tensile stress occurs in

the upper right (90 ~ 180°) direction. This is because of the stress concentration at the crack tip caused by the root opening. In (c), the shear stress distribution is almost reversed regardless of whether the root is open or closed.

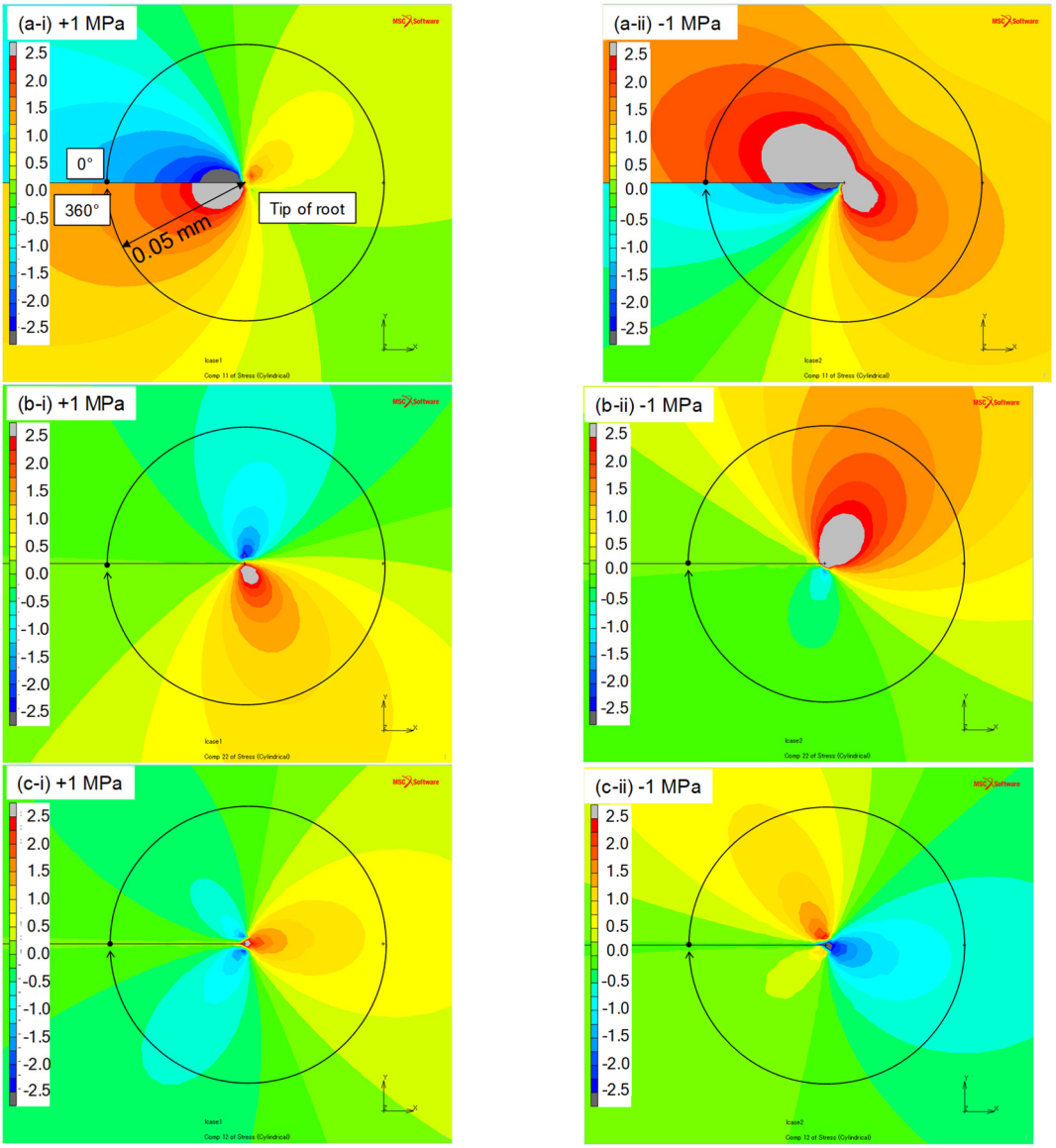

Figure 6. Stress contours around the root area (M6): (a) radial stress, (b) circumferential stress, and (c) shear stress.

The radial, circumferential, and shear stress distributions at a radius of 0.05 mm from the origin were obtained. **Figure 7** shows the difference in stress (stress range)

between the bending stresses of -1 MPa and +1 MPa for each stress component. (a) shows a schematic diagram of the stress obtaining position. In (b), it is observed that the radial stress range is larger around 0° and 360°. This might be because of the change in the bending stress of the base material. In (c), it is seen that the circumferential stress range is larger in the direction from 90° to 180°, with a maximum value in the direction of 110°. The stress range for M8 is lower than that for M6. The difference in stress ranges is 5.4%. From (d), it is inferred that the shear stress range has a maximum in the 180° direction, which coincides with the direction of the sheet interface.

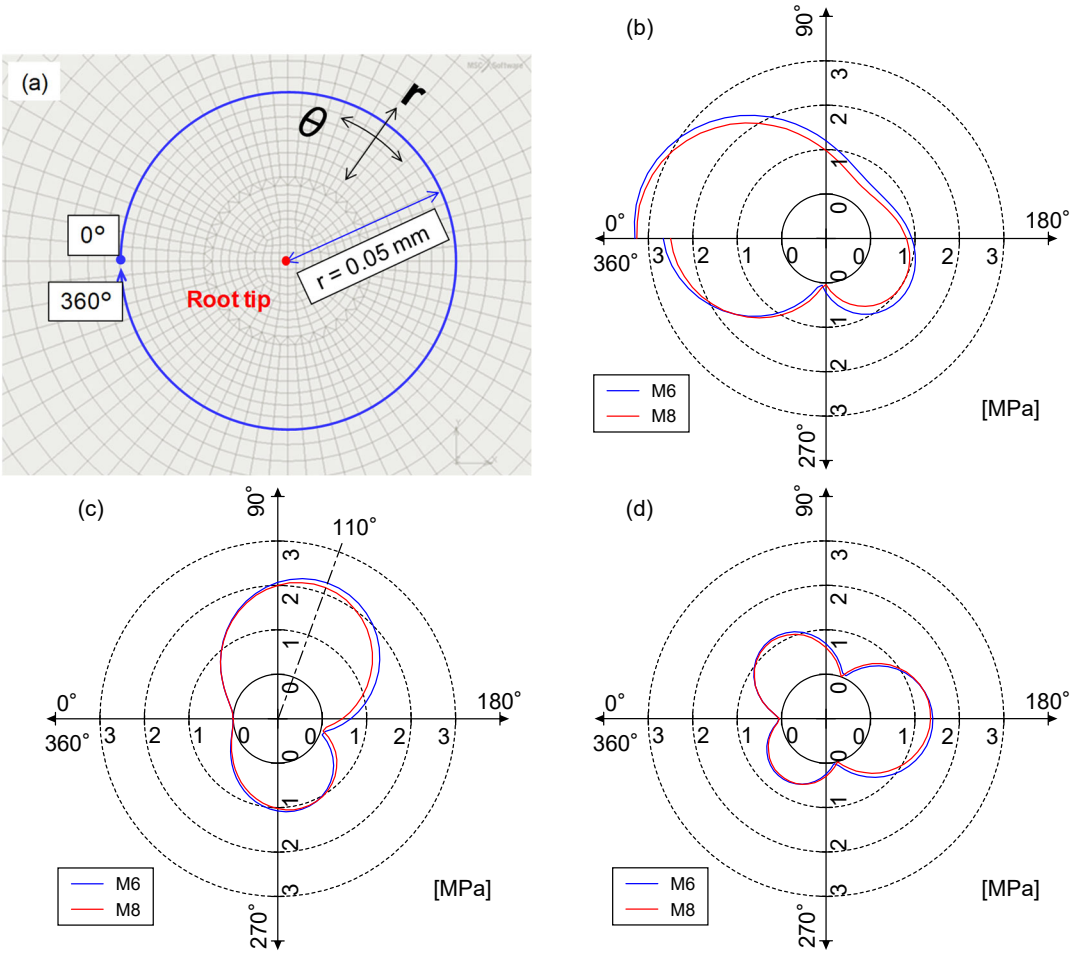

Figure 7. Stress distribution at r=0.05: (a) schematic of stress obtaining location, (b) radial stress, (c) circumferential stress, and (d) shear stress.

4.2 Experiment

Figure 8 shows a cross-sectional image of the weld. The weld penetration width was slightly longer than the target, 6.3 mm for S and 8.4 mm for L. The height of excess weld metal of L was higher than that of S.

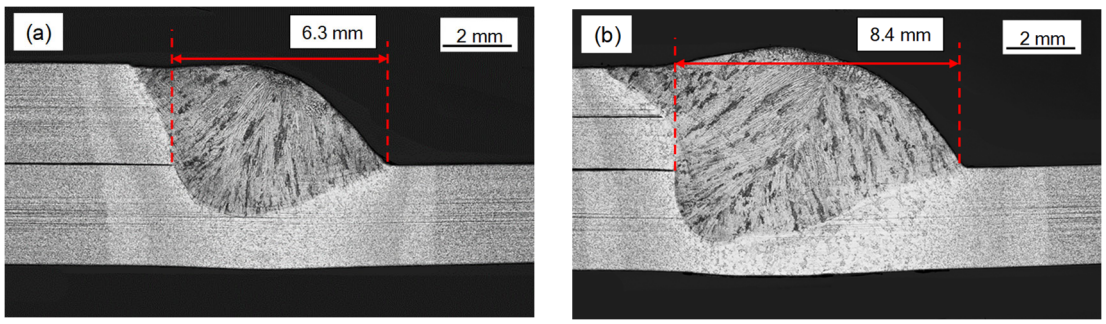

Figure 8. Cross-sectional image of the weld: (a) S and (b) L.

The S-N diagram obtained from the fatigue tests is shown in Figure 9. The fatigue limit of L was about 60 MPa higher than that of S.

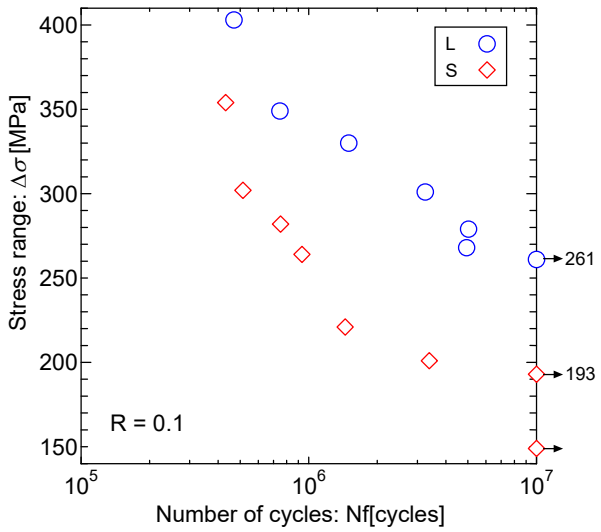

Figure 9. S-N diagram.

Figure 10 shows a cross-sectional image of a fatigue crack examined in the central cross-section of a specimen that had not failed at 10^7 cycles. Figure 10 shows a circle with a radius of 50 μm from the root tip and the direction of crack propagation as in Figure 7. In both cases, the crack propagated slightly in the direction of 180° along the sheet interface, and then in the direction of 118° in the case of S and in the direction of 128° in the case of L.

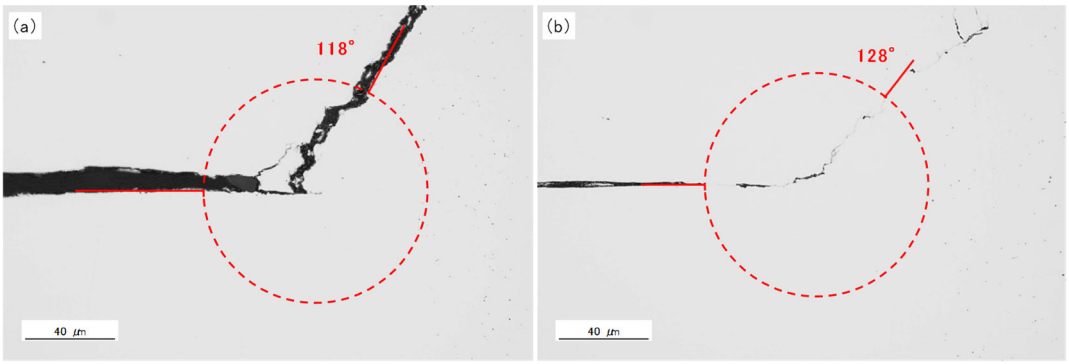

Figure 10. Fatigue cracks in the root section: (a) S and (b) L.

5. Discussion

According to [12], the direction of fatigue crack propagation under combined loading is the direction of maximum circumferential stress range $\Delta\sigma_\theta$ for Mode I (crack opening type) and the direction of maximum shear stress range $\Delta\tau_{r\theta}$ for Mode II (in-plane shear type). Furthermore, whether the crack propagates in Mode I or Mode II is determined by the crack propagation rate, da/dN, obtained from the stress intensity factor ranges ΔK_I and ΔK_{II} [13]. As shown in Figure 10, the direction along which the fatigue crack at the root tip propagates is known. By comparing the direction of crack propagation with the direction of maximum circumferential and shear stress ranges, it is possible to determine whether the fatigue crack propagates in Mode I or Mode II at the root.

Figure 10 shows that the fatigue cracks at the root of the lap fillet weld propagated slightly in the direction of 180° from the root tip. This is consistent with the

direction of the maximum shear stress range in Figure 7 (d). During this period, the fatigue crack propagated in Mode II. The direction of crack propagation in Figure 10 (a) coincided with the direction of maximum circumferential stress range in Figure 7 (c) under the 6 mm penetration width condition. Murakami et al. [14] reported that the fatigue limit under shear stress in torsion is the limit of Mode I fatigue crack propagation. The fatigue limit in this test is also the propagation limit of the fatigue crack after the crack transition to Mode I. In other words, the circumferential stress component is considered to be dominant for the root fatigue strength.

In contrast, Figure 7 (c) shows that the circumferential stress is reduced in the model with a penetration width of 8 mm. The parameter that controls the fatigue crack propagation rate is the stress intensity factor range ΔK [15]. The parameter that controls the fatigue crack propagation rate in Mode I under combined loading mode is ΔK_θ. The stress intensity factor range is the difference between the stress intensity factor K at maximum and minimum loading. In the present model, the stress singularity disappears at the minimum load because the root closes, and the value of K is zero. Therefore, the K value when the root opens (at a bending stress of -1 MPa) is the equal to ΔK. The K_θ values at the root tip are shown in Table 2. In this analysis, the J-integral values were calculated by area integration according to MSC. Marc, and converted to stress intensity factor. Table 2 shows that the K value increases with decreasing penetration width.

The stress intensity factor obtained in Table 2 are converted into stresses at the fatigue limit. The root section is supposed to be a crack due to high stress concentration, and the fatigue limit is postulated to depend on ΔK_{th}, which is the limit of propagation of fatigue cracks. From the test results shown in Figure 9, if the fatigue limit of M6 is 193 MPa, the ΔK_{th} corresponding to the fatigue limit is 3.34 [MPa$\sqrt{}$m]. The error of this estimation result with the fatigue limit of L obtained by the fatigue test is about 13%, which is a reasonable accuracy. One of the reasons for the error is that the penetration width in the FE analysis is slightly different from the actual penetration width of the weld. As another factor, Figure 8 (b) shows that the throat thickness of L is larger than that of S and is larger than the top edge of the upper sheet. This may have changed the stress state at the root. As a corollary, Figure 10 (b) shows that the direction of fatigue crack propagation in L is at an angle greater than 110°. The effect of the throat thickness will be studied in the future.

Table 2. Summary of stress intensity factor and estimated fatigue limit

	$K_{\theta max}$	$\Delta K_{\theta th}$	Fatigue limit	Estimation	Error
	$(\times 10^{-2})$ MPa√m		MPa	MPa	%
M6 (S)	1.73	3.34	193	-	-
M8 (L)	1.47		261	**227**	**-13.0**

6. Conclusion

The dominant factors of fatigue strength at the root of sheet lap fillet arc welds, widely used in automotive chassis components, were investigated. In addition, a fatigue strength improvement method using the root as the crack initiation point was investigated. The results are described below.

- The direction of fatigue crack propagation at the root coincided with the direction of maximum circumferential stress range in the polar coordinate system with the root tip as the origin.
- The circumferential stress could be reduced by increasing the distance from the toe to the root (penetration width).
- It was confirmed that the fatigue strength of the weld joint root was improved by increasing the penetration width through adjustment of the weld aim point and heat input.

Acknowledgments

Authors are deeply grateful to Mr. Miyake, Mr. Narukawa, Mr. Sato, and others of Nippon Steel Technology Co., Ltd., for support in the experimental and analytical work.

Funding

This research did not receive any specific grant from funding agencies in the public, commercial, or not-for-profit sectors.

References

[1] Duchet M, Haouas J, Gibeau E, Pechenot F, Honecker C, Munier R. Improvement of the fatigue strength of welds for lightweight chassis application made of Advanced High Strength Steels. Proc. Struct. Integr. 2019; 19: 585–94. https://doi.org/10.1016/j.prostr.2019.12.063

[2] Ahiale GK, Oh Y-J. Microstructure and fatigue performance of butt-welded joints in advanced high-strength steels. Mat. Sci. Eng. A 2014; 597: 342-348. https://doi.org/10.1016/j.msea.2014.01.007

[3] Kodama S, Ishida Y, Furusako S, Saito M, Miyazaki Y, Nose T. Arc Welding Technology for Automotive Steel Sheets. Nippon Steel Tech Rep 2013; 103: 83-90.

[4] Matsuda K, Kodama S. Observation of fatigue microcracks and estimation of fatigue strength of a thin sheet arc welded part considering micro-ripples. Int. J. Fatigue 2021; 145: 106087. https://doi.org/10.1016/j.ijfatigue.2020.106087

[5] Shiozaki T, Yamaguchi N, Tamai Y, Hiramoto J, Ogawa K. Effect of weld toe geometry on fatigue life of lap fillet welded ultra-high strength steel joints. Int. J. Fatigue 2018; 116: 409–20. https://doi.org/10.1016/j.ijfatigue.2018.06.050.

[6] Fujimoto H, Akioka K, Tokunaga M. Effects of Shot Blasting on Corrosion Properties after Electrodeposition and Fatigue Properties of Arc Welds in Automotive Steel Sheets. Mater. Trans. 2017; 58(12): 1715–20. https://doi.org/10.2320/matertrans.P-M2017838.

[7] Yamaguchi N, Shiozaki T, Tamai Y, Okuda K, Ichikawa Y, Ogawa K. Effect of cold spray deposition on fatigue strength of arc-welded ultra-high strength steel sheet. Int. J. Fatigue 2022; 161, 106876. https://doi.org/10.1016/j.ijfatigue.2022.106876.

[8] Fricke W, IIW guideline for the assessment of weld root fatigue, Weld World 2013; 57: 753-791. https://doi.org/10.1007/s40194-013-0066-y

[9] Fricke W, Kahl A, Paetzold H. Fatigue assessment of root cracking of fillet welds subject to throat bending using the structural stress approach. Weld World 2006; 50: 64–74. https://doi.org/10.1007/BF03266538

[10] Meneetti G., Campagnolo A., State-of-the-art review of peak stress method for fatigue strength assessment of welded joints. Int. J. Fatigue, 2020, 139, 105705. https://doi.org/10.1016/j.ijfatigue.2020.105705.

[11] Song W, Liu X, Berto F, Wang P, Xu J, Fang H. Strain energy density based fatigue cracking assessment of load-carrying cruciform welded joints. Theor. Appl. Fract. Mech. 2017; 90: 142-153. https://doi.org/10.1016/j.tafmec.2017.04.002

[12] Tanaka K, Akiniwa Y, Kato T, Mikuriya T. Fatigue crack propagation from a precrack under combined torsional and axial loading. Fatigue Fract. Eng. Mater. Struct. 2005; 28: 73–82. https://doi.org/10.1111/j.1460-2695.2005.00861.x

[13] Pinna C, Doquet V. The preferred fatigue crack propagation mode in a M250 maraging steel loaded in shear. Fatigue Fract. Eng. Mater. Struct. 1999; 22: 173–183. https://doi.org/10.1046/j.1460-2695.1999.00161.x

[14] Murakami, Takahasi. Torsional Fatigue of a Medium Carbon Steel Containing an Initial Small Surface Crack Introduced by Tension–Compression Fatigue: Crack Branching, Non－Propagation and Fatigue Limit. Fatigue Fract. Eng. Mater. Struct. 1998; 21: 1473–1484. https://doi.org/10.1046/j.1460-2695.1998.00128.x

[15] Frost NE, Pook LP, Denton K. A fracture mechanics analysis of fatigue crack growth data for various materials. Eng. Fract. Mech. 1971; 3: 109-126. https://doi.org/10.1016/0013-7944(71)90003-8